PHYSICAL REVIEW D

PARTICLES AND FIELDS

THIRD SERIES, VOL. 7, NO. 7 1 April 1973

# Three-Body Decays of $K^0$ Mesons*

M. L. Mallary, D. M. Binnie,† J. D. Gallivan,‡§ R. Gomez, C. W. Peck, F. J. Sciulli, B. A. Sherwood,‖ A. V. Tollestrup, and J. D. Van Putten**
*California Institute of Technology, Pasadena, California 91109*
(Received 9 June 1972)

We have measured the time distributions of the $\pi^+e^-\bar{\nu}$, $\pi^-e^+\nu$, and $\pi^+\pi^-\pi^0$ modes from initially pure $K^0$'s in a spark-chamber experiment performed at the Bevatron. From 1079 $K_{e3}$ events between 0.2 and 7 $K_S$ lifetimes, we find $\mathrm{Re}X = -0.070 \pm 0.036$, $\mathrm{Im}X = 0.107^{+0.092}_{-0.074}$. This result is consistent with $X = 0$ (relative probability = 0.25). From 148 $K \to \pi^+\pi^-\pi^0$ events in the same fiducial volume, we get $\mathrm{Re}W = -0.05 \pm 0.17$ and $\mathrm{Im}W = 0.39^{+0.35}_{-0.37}$. ("$W$" is variously known as $\eta^{+-0}$ and $x + iy$.) Our results are consistent with $W = 0$ (relative probability = 0.30).

## I. INTRODUCTION

The observation of the decays[1] $K_L^0 \to \pi^+\pi^-$ and of interference between $K_S^0$ and $K_L^0$ decays into $2\pi$ provides convincing evidence of $CP$ violation with an amplitude of about $2\times10^{-3}$ of the $CP$-conserving part. Present evidence[2] is consistent with the assumption that the effect arises from physical $K_S^0$ and $K_L^0$ states which are not eigenstates of $CP$. Under this assumption, the Hamiltonian which determines the eigenstates of the $K^0, \bar{K}^0$ system is not invariant under $CP$. There have been numerous theoretical conjectures[3] regarding the origin of the $CP$ violation, ranging from a "superweak" interaction with a coupling constant of about $10^{-8}$ of the weak coupling all the way to a maximal violation in the electromagnetic interactions.

One class of theories[4,5] would require a large (or maximal) violation in the three-body $K^0$ decays. For the leptonic decays,

$$K^0 \to \pi^+ + e^- + \bar{\nu}, \tag{1a}$$

$$\bar{K}^0 \to \pi^+ + e^- + \bar{\nu}, \tag{1b}$$

$$\bar{K}^0 \to \pi^- + e^+ + \nu, \tag{1c}$$

$$K^0 \to \pi^- + e^+ + \nu, \tag{1d}$$

there are (assuming $CPT$ invariance) two complex amplitudes: Reactions (1b) and (1d) proceed through a $\Delta S = \Delta Q$ transition, while (1a) and (1c) through a $\Delta S = -\Delta Q$ transition. If we define $X_-$ = ratio of amplitudes for reactions (1a)/(1b), and $X_+$ = ratio of amplitudes for reactions (1c)/(1d), then $CPT$ invariance requires

$$X_+ = X_-^*.$$

Of course, the selection rule $\Delta S = \Delta Q$ predicts $X_+ = X_- = 0$. A maximal $CP$ violation[4] in the leptonic decays would have $|\mathrm{Im}X| \simeq 1$.

The three-body pion decays which we shall consider,

$$K^0 \to \pi^+ + \pi^- + \pi^0 \tag{2a}$$

$$\bar{K}^0 \to \pi^+ + \pi^- + \pi^0, \tag{2b}$$

primarily occur with final states of total isotopic spin $I = 1$. This is due to centrifugal barriers impeding other states.[6] If we define the complex amplitude for reaction (2a) as $Ye^{i\varphi}$ and the amplitude for reaction (2b) as $-\bar{Y}e^{-i\bar{\varphi}}$, then $CPT$ requires $Y = \bar{Y}$ and $CP$ requires both $\varphi = \bar{\varphi}$ and $Y = \bar{Y}$. Cabibbo[7] has shown that, assuming $CPT$ invariance and the $|\Delta I| = \frac{1}{2}$ rule for nonleptonic decays, the rates for $K_L^0$ and $K_S^0$ decay are, approximately,

$$\Gamma(K_L^0 \to \pi^+\pi^-\pi^0) = \tfrac{1}{2}P\Gamma(K^+ \to \pi^+\pi^+\pi^-)\cos^2[\tfrac{1}{2}(\varphi - \bar{\varphi})], \quad (3a)$$

$$\Gamma(K_S^0 \to \pi^+\pi^-\pi^0) = \tfrac{1}{2}P\Gamma(K^+ \to \pi^+\pi^+\pi^-)\sin^2[\tfrac{1}{2}(\varphi - \bar{\varphi})], \quad (3b)$$

where $P = \pi^+\pi^-\pi^0/\pi^+\pi^+\pi^-$ phase-space ratio.

Using recent data[8] on the $K_L^0, K^+$ decay rates, Eq. (3a) gives $\varphi - \bar{\varphi} = 50° \pm 6°$, predicting

$$\frac{\Gamma(K_S^0 \to \pi^+\pi^-\pi^0)}{\Gamma(K_L^0 \to \pi^+\pi^-\pi^0)} = 0.150^{+0.017}_{-0.023}.$$

If the discrepancy between the $K_S$ and $K^+$ rates is really due to $CP$ violation (and not to a small $|\Delta I| = \frac{3}{2}$ amplitude), the magnitude is similar to the maximal $CP$ violation described by Glashow.[5]

In this experiment we have produced $K^0$'s by associated production and observed their decays as a function of time. Neglecting terms of order $\epsilon$,[9] the time distribution for leptonic decays is expected to be (+ is for positive electrons)

$$F^{\pm}(t) = |1 + X_{\pm}|^2 e^{-t/\tau_S} + |1 - X_{\pm}|^2 e^{-t/\tau_L} \pm [2(1 - |X_{\pm}|^2)\cos\Delta m t - 4\,\mathrm{Im}X_{\pm}\sin\Delta m t]\exp\left[-\tfrac{1}{2}t\left(\frac{1}{\tau_S} + \frac{1}{\tau_L}\right)\right], \quad (4)$$

while the time distribution for $3\pi$ decays is

$$F^{3\pi}(t) = |W|^2 e^{-t/\tau_S} + e^{-t/\tau_L} + 2[(\mathrm{Re}W)\cos\Delta m t - (\mathrm{Im}\,W)\sin\Delta m t]\exp\left[-\tfrac{1}{2}t\left(\frac{1}{\tau_S} + \frac{1}{\tau_L}\right)\right], \quad (5)$$

where $\Delta m = m_L - m_S$, $\tau_S$ and $\tau_L$ are the lifetimes of $K_S^0$ and $K_L^0$, respectively, and

$$W = \frac{\langle 3\pi | H_w | K_S \rangle}{\langle 3\pi | H_w | K_L \rangle} \quad (6)$$

Neglecting terms of order $\epsilon$,

$$\mathrm{Re}W = \frac{|Y|^2 - |\bar{Y}|^2}{|Ye^{i\varphi} + \bar{Y}e^{-i\varphi}|^2}$$

and

$$\mathrm{Im}W = \frac{+2Y\bar{Y}\sin(\varphi - \bar{\varphi})}{|Ye^{i\varphi} + \bar{Y}e^{-i\varphi}|^2}.$$

Therefore, to order $\epsilon$, $CPT$ invariance requires $\mathrm{Re}W = 0$ while $CP$ invariance requires $W = 0$ (assuming that the $I = 1$ $3\pi$ state is dominant).

## II. THE APPARATUS

The decay distributions for $K^0 \to \pi^\mp e^\pm \nu$ and $K^0 \to \pi^+\pi^-\pi^0$ were measured using the apparatus shown in Fig. 1. Events of the two types were collected simultaneously using two different counter trigger requirements. Separate runs were also made with a trigger designed to favor $K^0 \to \pi^+\pi^-$ events for the purpose of calibrating the apparatus and determining the $K^0$ beam momentum and angular distribution. (See Sec. V.)

### The $K^0 \to \pi^+\pi^-$ Trigger

The $K^0$ particles used in this experiment were produced in two brass targets (target detail shown in Fig. 1) by the reaction $\pi^- + P_{\text{brass target}} \to \Lambda^0 + K^0 + \text{other}$. The $\pi^-$ beam originated on an internal target at zero degrees in the LBL Bevatron. Its momentum was 2.85 GeV/$c$. After passing through upstream counters $S1$, $S2$, $S3$, the $\pi^-$ beam entered the production-decay region of the apparatus (Fig. 1) through beam counter $S4$ and a hole in the beam veto counter $S4V$. After passing through $S4$, the beam traversed an optical spark-chamber module. It then entered the first target ($T1$) triggering counter $C_1$. A neutral trigger was signaled by the requirement $C_1 * \bar{V}_1$. That is, the $\pi^-$ interacted in $T1$ without producing forward charged secondaries that would trigger $V_1$. One third of the pions that did not interact in $T1$ (10% interacted) would subsequently strike $T2$ (24 in. downstream), where they might interact to satisfy its trigger requirement ($C_2 * \bar{V}_2$). The two-target configuration was chosen to get as many $K \to \pi e \nu$ events as possible at early lifetimes, where $F^-(t)$ is sensitive to $X$. Even though $T2$ received only $\frac{1}{3}$ the beam of $T1$, the high event acceptance from $T2$ caused it to produce as many accepted early lifetime events as $T1$. The mean $K^0$ momentum accepted by the apparatus was 2.4 GeV/$c$. There were 6 spark chamber modules downstream of $T1$ and 2 downstream of $T2$. This allowed the $K^0$ about 7 and 2 $K_S$ lifetimes, respectively, in which to decay.

Figure 1 illustrates a typical $\pi^+\pi^-$ event in the apparatus. The $K^0$ which was produced in $T1$ travels to a point where it decays into two charged secondaries (dashed lines). As the $\pi^+$ and $\pi^-$ fan out from the decay point they leave a "vee" in the optical spark chambers of the decay region. At the end of this region one of them must trigger counter $S5$. This counter defines the entrance aperture to the momentum spectrometer region and determines that the neutral which was produced in one of the targets has decayed in the decay region. $S5$ was a

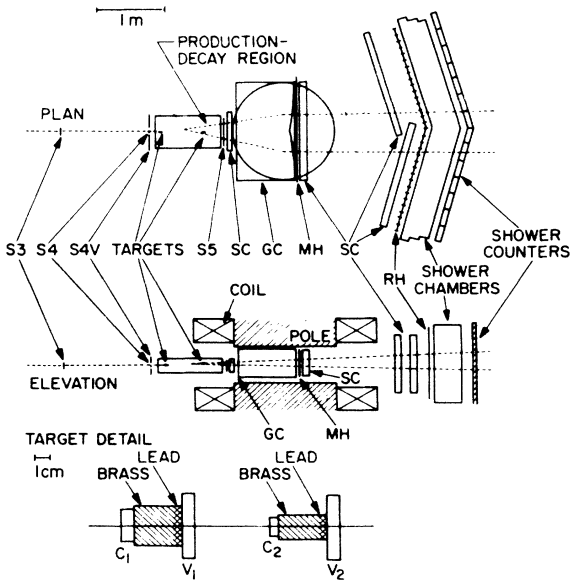


FIG. 1. Experimental apparatus: $S3$, $S4$, beam counters; $\overline{S4V}$, beam veto counter; $S5$, counter defines the end of the decay region; $SC$'s, thin plate spark chambers; GC, gas Čerenkov counter; MH, hodoscope with 15 horizontally oriented counters; RH, hodoscope with 32 vertically oriented counters; shower spark chambers, 18 plates with a total of 2.7 radiation lengths; shower counters (vertical orientation), 14 counters with two radiation lengths of lead between two slabs of scintillator; targets (below), three centimeters of brass followed by two millimeters of lead; $C_i$, counter in front of target $i$ demands incoming beam particle; $V_i$, veto counter in back of target $i$ demands no charged, forward secondaries.

$\frac{1}{8}$-in.-thick scintillator to minimize triggers caused by neutron stars and $\gamma$ conversion in its material. Each of the 7 spark chamber modules in the production-decay region had 0.01 radiation lengths of material, most of which was aluminum foil.

After passing through $S5$, the two charged secondaries traversed the first spark chamber module of the momentum spectrometer region. They then entered the gas Čerenkov counter where they traversed ~30 in. of Freon-12 at a pressure of 1 atm. Under these conditions the momentum thresholds for electrons, muons, and pions are 0.01, 2.3, and 3.0 GeV/$c$, respectively. This counter had an efficiency of >97% for detecting electrons. This efficiency was independent of the decay point (in the production-decay region) to 1.2%. The pion rejection ratio was $(69 \pm 7)$ to 1. The Čerenkov light was viewed by two optical systems, one on each side at the center line. The phototube pulse height for each system was part of the recorded data. The Čerenkov counter, however, was not included in the $K \to \pi^+\pi^-$ trigger.

Directly downstream of the rear window of the Čerenkov counter, near the center of the magnet, the two charged secondaries passed through the multiples hodoscope (MH). This hodoscope consisted of 15 scintillators 60 in. long, 1 in. wide, and $\frac{3}{8}$ in. thick oriented with their length horizontal and their width vertical. The trigger requirement of this hodoscope was that exactly 2 counters trigger, indicating two charged secondaries. The two triggered counters had to be separated by at least one counter that did not trigger. Directly behind this hodoscope was a spark chamber.

On leaving the rear of the spectrometer magnet, the secondaries traversed another spark chamber (2 chambers, one on each side of the apparatus) and then passed through the rear hodoscope (RH). This hodoscope had a total of 32 counters which were in two banks of 16. The normal to each bank was at 16° to the beam line so that the average secondary trajectory was perpendicular to it. This was also the case for the chambers directly in front of this hodoscope as well. Each of the 32 counters was 42 in. high, 4 in. wide, and $\frac{3}{8}$ in. thick. The $K^0 \to \pi^+\pi^-$ trigger requirement for this hodoscope was that exactly 2 counters trigger. This further reinforced the two-particle requirement of the multiples hodoscope.

Next the charged secondaries entered the shower region of the apparatus. First they passed through the shower chambers. These chambers had 18 $\frac{3}{8}$-in. gaps. The total material presented to an incident particle was 1.08 in. of aluminum and 0.54 in. of lead for a total of 2.7 radiation lengths and 0.2 collision lengths of material. Again, the normal to the chambers on each side of the center line was at 16° to the center line.

Directly behind the shower chambers were the shower counters. They consisted of 14 counters in two groups. Each counter was 52 in. high and 10 in. wide, and consisted of 2 radiation lengths of lead sandwiched between two $\frac{3}{8}$-in.-thick scintillators. Each scintillator was connected to one phototube. In order to minimize the attenuation effects, the two tubes were connected at opposite ends of the sandwich and their pulses were added electronically. The pulse height for each of the 14 counter pairs was part of the data recorded on magnetic tape. Once again, the shower counters were not included in the $K^0 \to \pi^+\pi^-$ trigger.

In summary, the $K^0 \to \pi^+\pi^-$ trigger counters $S1$, $S2$, $S3$, and $S4$ in coincidence and $S4V$ in veto to define the $\pi^-$ beam. Next, the coincidence counter in one of the targets had to trigger without the corresponding veto counter, indicating an interaction with no charged forward secondary. Next,

$S5$ had to trigger to indicate charged forward secondaries from a neutral decay entering the magnet. Then the multiples hodoscope and the rear hodoscope each had to have two triggered counters indicating two and only two charged secondaries in the spectrometer.

### The $K^0 \to \pi^+ e^\mp \nu$ Trigger

This trigger was similar to the $K^0 \to \pi^+\pi^-$ trigger, but it had one additional requirement: The gas Čerenkov counter described above had to produce a pulse above a very low threshold. The requirement on the multiples hodoscope that the two counters which triggered be separated from each other by at least one counter (1 in.) was the same as in the $K^0 \to \pi^+\pi^-$ trigger. This demanded that the events have opening angles in excess of one degree, removing much of the triggering background due to $e^+e^-$ pairs.

### The $K^0 \to \pi^+\pi^-\pi^0$ Trigger

This trigger differed from the $K^0 \to \pi^+\pi^-$ trigger in three respects. First, the triggered counters were required to be on separate sides of the rear hodoscope array. Next, the sum of the pulse heights in the shower counters on either side (7 counters in each sum) of the center line had to exceed the pulse of a 3 times minimum-ionizing track. This requirement, in conjunction with the previous one, was designed to bias towards accepting events with an associated $\gamma$ ray. Finally, the two triggered multiples-hodoscope counters did not have to be separated from each other. The separation requirement was dropped because charged tracks in $K^0 \to \pi^+\pi^-\pi^0$ events have somewhat smaller opening angles than $K^0 \to \pi^+\pi^-$ events.

### Data Recording

The optical spark-chamber data were recorded with 3 Flight Research cameras on 35 mm double frames. For each region of the apparatus (production-decay, momentum spectrometer, and the shower regions in Fig. 1), there was a separate optical system and a separate camera. There were $5\times10^4$, $2.4\times10^5$, and $2.7\times10^5$ pictures taken for the $K^0 \to \pi^+\pi^-$ mode, the $K^0 \to \pi^\pm e^\mp \nu$ mode, and the $K^0 \to \pi^+\pi^-\pi^0$ mode, respectively. The digital counter information (which counters triggered), the pulse-height information for each side of the gas Čerenkov counter, and the 14 shower counters were recorded on magnetic tape for each event. This was done with the aid of an on-line PDP-8 computer which also stored and displayed histograms for monitoring the performance of the apparatus.

## III. DATA REDUCTION

### $K^0 \to \pi^\pm e^\mp \nu (K_{e3})$

The first step in isolating the 1079 final $K_{e3}$ triggers was a computer examination of the magnetic data tape. First of all, events inconsistent with the fast-trigger logic were filtered out. Then, selection criteria were applied to the shower-counter pulse heights; the two groups of shower counters directly downstream of the two triggered rear hodoscope counters were examined for an electron pattern and a pion pattern. The electron pattern required that the sum of the pulses in two adjacent shower counters in the group had to be greater than 1.7 minimum-ionizing. The pion pattern required that one and only one counter in the group had to have a pulse ranging from 0.5 to 2.6 minimum-ionizing. The shower-counter criterion then was that there be an electron pattern in one group and a pion pattern in the other. If the two triggered rear hodoscope counters were separated by less than five counters then only the electron pattern was required. After this stage of the reduction, 67 205 candidate events remained. On the basis of 524 $K_{e3}$ events obtained without the pulse-height selections, it is estimated that this process was at least 75% efficient at selecting real events. The fraction missed in the computer scan showed no bias dependent on vertex positions of the decaying vee.

The next step in the $K_{e3}$ data reduction was a visual scan of the shower chambers. Accepted events had to have one pion and one electron, each of which extrapolated to within $\frac{1}{2}$ a counter of one of the triggered rear hodoscope counters. Events with extra tracks which extrapolated into these counters were rejected. Events without a visible shower ($\pi\pi$ events) and events with two visible showers ($ee$ events) were rejected. The $\pi\pi$ events were carried through the analysis, however, for calibration purposes. Pion interactions were distinguished from electron showers on the basis of whether or not there was a well-defined interaction vertex. Using an independently scanned sample of events it is estimated that this stage of the reduction was 96% efficient at retaining events that met the criteria. The number of candidate events left after this step was 14 613. Most of the rejected events were electron pairs.

The next step in the reduction process was a visual scan of the production-decay region for 2-prong neutral vees. In order to prevent scanning inefficiencies from biasing the position distribution of the decays, this scan was done independently by two different scanners. If either scanner found a vee, it was accepted. When their results were

compared they were found to be individually 97% efficient at finding vees. The events which were missed showed no position bias relative to the accepted events. The scanners noted the vertex positions from a template and any discrepancies of greater than 1 in. in real space were examined by a physicist.

The production-decay region scan began with a search for two tracks in the elevation view which extrapolated to the two multiples hodoscope counters involved in the trigger. $T1$ tracks had to extrapolate to within two counters of a triggered counter and $T2$ tracks to within three. Next, the two tracks were required to form a vertex. The longitudinal positions of the vertex in the two views (elevation and plan) had to be visually consistent with each other to 1 in. If a third track entered or left the vertex it was rejected. Vees that passed through two or more spark chamber modules (out of a possible six) without opening (separating into two distinguishable tracks) were rejected. This was equivalent to rejecting events with opening angles less than 2°. This rejected most electron pair events, but did not seriously affect the $K_{e3}$ events. (Monte Carlo calculations indicated that this cut removes about 0.1% of the $K_{e3}$ data.) In addition, if either prong of the vee had a kink of more than 5° the event was rejected. After this scan 3395 event candidates remained.

The pictures which passed the above scans were then measured in the production-decay region and the shower region. Candidates at this stage contained a vee in the production-decay region and an electron and hadron in the shower region. It remained to choose those events in which these tracks were continuous. The elevation positions in the two regions were used to construct a straight line through the apparatus for each track. If these two lines missed the two triggered MH counters by more than one counter (1 in.) the event was rejected. 23% of the events were rejected for this reason. The remaining events were fitted to trajectories through the magnet and a vertex in the decay region using the angles and positions as measured in the shower and the production-decay regions. If the $\chi^2$ for either track exceeded 100 ($\langle\chi^2\rangle = 4$) the event was rejected. This $\chi^2$ cut removed 11% of the candidates. The remaining 2226 events were then measured in the momentum spectrometer region. New fitted trajectories were calculated using all the spark chamber measurements which were consistent with the first calculated trajectory (the moment resolution for this fit was $\Delta p/p \approx 0.05$). Then a series of consistency cuts were made on the events. The $\chi^2/\nu$ was required to be less than 5 for each track; the charges were required to be opposite; the momentum of each track was required to be less than 4 GeV/$c$; each trajectory had to be within $\frac{1}{2}$ a counter of its rear hodoscope counter and its multiples hodoscope counter; the electron had to have a shower counter pulse greater than 1.2 minimum-ionizing; and the pulse heights in the two sides of the gas counter had to be consistent with the electron trajectory. These cuts reduced the sample to 1691 events. 86% of the 535 rejected events violated more than one criterion.

The events which reconstructed well were then reexamined in the shower region and the production-decay region by a physicist. The scanner had been instructed to accept any doubtful events, so there was room for a more stringent application of the scanning criteria. In addition, the added information of the trajectory parameters and the pulse heights made it possible to resolve certain ambiguities. After this rescan, 1337 event candidates remained. 85% of these 354 rejects were removed by the rescan of the shower chamber picture.

After the rescan a final group of cuts was applied to the data, primarily to remove backgrounds from $\gamma \to e^+e^-$ and $\Lambda^0 \to pe^-\nu$. (See Sec. IV.) An electron-proton ($M_{ep}$) invariant mass was calculated assuming that the pion was a proton (for both charges of the pion). This mass was required to be greater than 1.115 GeV. This removed 163 events, $19 \pm 6$ of which were estimated to be true $\Lambda$-$\beta$ decays. The $e$-pair mass (assumes the pion is an electron) was required to be greater than 0.030 GeV, removing 8 events. This cut should remove 97% of the $e$-pair events resulting from $\gamma$ conversion in the spark chamber's foil plates. Finally, 86 events were removed with a fiducial volume cut. This cut excluded events that decayed in the first plate behind each target, reinforcing the target veto counter requirement, and also removed events in the last 2 in. of the decay region (minimum track length was 2 in. or 5 sparks). The final sample of $K_{e3}$ events then consisted of 1079 events.

$$K^0 \to \pi^+\pi^-\pi^0 (K_{\pi 3})$$

The sequence for the $K^0 \to \pi^+\pi^-\pi^0$ data reduction was very similar to that for the $K^0 \to \pi e \nu$ events. There were $2.7\times10^5$ $K^0 \to \pi^+\pi^-\pi^0$ pictures taken. This was reduced to $1.5\times10^5$ pictures from the start by taking only the $T1$ events. $T2$ events would be more susceptible to background, and improve the sensitivity of the experiment only slightly.

A computer scan was performed which reduced the data sample to 17 234 pictures, retaining $K \to \pi^+\pi^-\pi^0$ events with 75% efficiency. The criteria again contained consistency requirements be-

tween the fast logic trigger and the information stored on magnetic tape. In addition, it was required that there be a pion pattern in the shower counters for each of the two triggered rear hodoscopes and at least one photon-shower pattern. The pion pattern consisted of a pulse greater than half minimum ionizing in either of two shower counters downstream of the triggered rear hodoscope counter. The showering photon pattern was a pulse greater than 1.2 times minimum ionizing in any of the shower counters that were not reserved for the pion pattern. The showering photon pattern had to occur on the same side of the shower counters as the large pulse which caused the original apparatus trigger.

The counters that satisfied the photon requirements were then examined in a visual scan of the shower chambers. The scanner first looked for a shower which would extrapolate into any of these shower counters. Specific visual evidence for a photon conversion was required. Each pion track (two) had to extrapolate to within one counter of its triggered rear hodoscope counter and had to produce at least three sparks in a row in the first of the three shower chamber modules. If more than one track extrapolated to a triggered rear hodoscope counter, the event was rejected. If either candidate pion was an obvious electron, the event was rejected. If the pion or any part of a pion interaction entered the photon shower counter, the event was rejected. Lack of a $\gamma$ ray was the principal reason for rejecting events. This visual scan of the shower chambers passed 4004 candidates. The scanners' efficiency was 95% on events meeting the criteria.

The next step in the data reduction was a visual scan of the production-decay region. First, two tracks were located in the elevation view which extrapolated into the triggered multiples hodoscope counters. The tolerances on this extrapolation were ±2 counters for tracks that were more than two spark chamber modules long (of a possible 6 modules) and 3 counters if the tracks were shorter than two modules long. These tracks then had to form vees whose vertices in the two views were consistent to about 2 in. in space. If a track had a kink of more than 5° the event was rejected. The scan was performed twice, by two independent scanners, who noted the positions of the vertex of the vees. If an event was accepted by one scanner and not by the other or if there was a discrepancy of greater than 1 in. in the observed vertex position then the event was examined by a physicist. The two scanners were individually 97% efficient at finding vees when they were compared to each other. This scan retained 2357 candidates.

At this point the events were measured and reconstructed in the same way as the $K \to \pi e \nu$ events, previously described. The same consistency cuts on the reconstructed trajectories were applied, leaving 1508 events.

The events which successfully reconstructed were then reexamined in the shower chambers by a physicist. 33% were rejected, leaving 1016 candidates. The principal reason for rejecting events in this rescan was that the $\gamma$ ray was caused by a pion interaction in the lead plates of the shower chambers.

Next the reconstructed tracks were required to satisfy certain geometric criteria. The $\chi^2/\nu$ for each track had to be less than 5. The tracks were required to have opposite curvature (opposite charges). Finally, each track had to pass through an appropriate aperture at the end of the production-decay region. These cuts passed 898 events.

The event candidates at this point consisted of three main types. These were $K^0 \to \pi^+\pi^-\pi^0$ events, $K^0 \to \pi^+\pi^-$ events with an associated $\gamma$ ray and $\Lambda^0 \to p\pi^-$ events with an associated $\gamma$ ray. The latter two types are backgrounds which had to be removed by kinematic cuts. The $\Lambda^0$ events were removed by assuming that the positively charged particle was a proton and the negative one was a pion in order to calculate a $\Lambda^0$ invariant mass. Events with masses less than 1.2 GeV were removed. The $K \to \pi^+\pi^-$ events were removed by assuming both tracks were pions and reconstructing the $2\pi$ mass. Events with a two-pion mass greater than 0.38 GeV were then removed. (See Sec. IV.) These two background cuts left 158 events in the $K \to \pi^+\pi^-\pi^0$ category. These were reduced to the final sample of 148 events by the same fiducial volume cut used in the $K_{e3}$ sample.

## IV. REMNANT BACKGROUND

### $K \to \pi^\pm e^\mp \nu$

The sources of background which have been considered as possibly significant in the $K_{e3}$ sample are shown in Table I with our best estimate of their size. The neutron star background might arise from neutrons produced in the targets and interacting with the material in spark chamber plates (0.003 collision lengths per module), although a resulting 2-prong neutral vee with one $\pi$ and one $e$ is unlikely. An upper limit for this background was estimated from the excess of $T1$ vees whose vertices lay in the target material of $T2$. On this basis, there are less than 5 such events in the entire sample.

The most significant source of background considered in designing the apparatus was the charged two-body decays of $K_S$ and $\Lambda$. These decays occur $10^3$ times more frequently than the $K_{e3}$ decays, thus

TABLE I. Backgrounds in the $K_{e3}$ sample.

| Type of background | Number present before cut | Cut imposed on final sample | Estimated background after cut |
|---|---|---|---|
| Neutron stars | <5 | No cut | <5 |
| $K_S \to 2\pi$, $\Lambda \to p\pi$ | 7.8 ± 10.0 | No cut | 7.8 ± 10.0 |
| Electron pairs | | | |
| (a) External conversions | ≤9 | $M_{e^+e^-} > 30$ MeV | ≤0.3 |
| (b) Dalitz pairs | 20 ± 5 | | 12 ± 3 |
| $\Lambda$ $\beta$ decay, $\Lambda \to p + e^- + \nu$ | 19 ± 6 | $M_{ep} > 1.115$ GeV | 0.0 |
| $\bar{K}^0$ production | | | |
| (a) $\pi^- p \to \bar{K}^0 K^0 n$ | <11 | | <11 |
| (b) $K^- p \to \bar{K}^0 n$ | ~5 ± 2 | | ~5 ± 2 |
| Total background in 1137 events | | | 25 ± 12; <11 from $\bar{K}^0 K^0$ production |

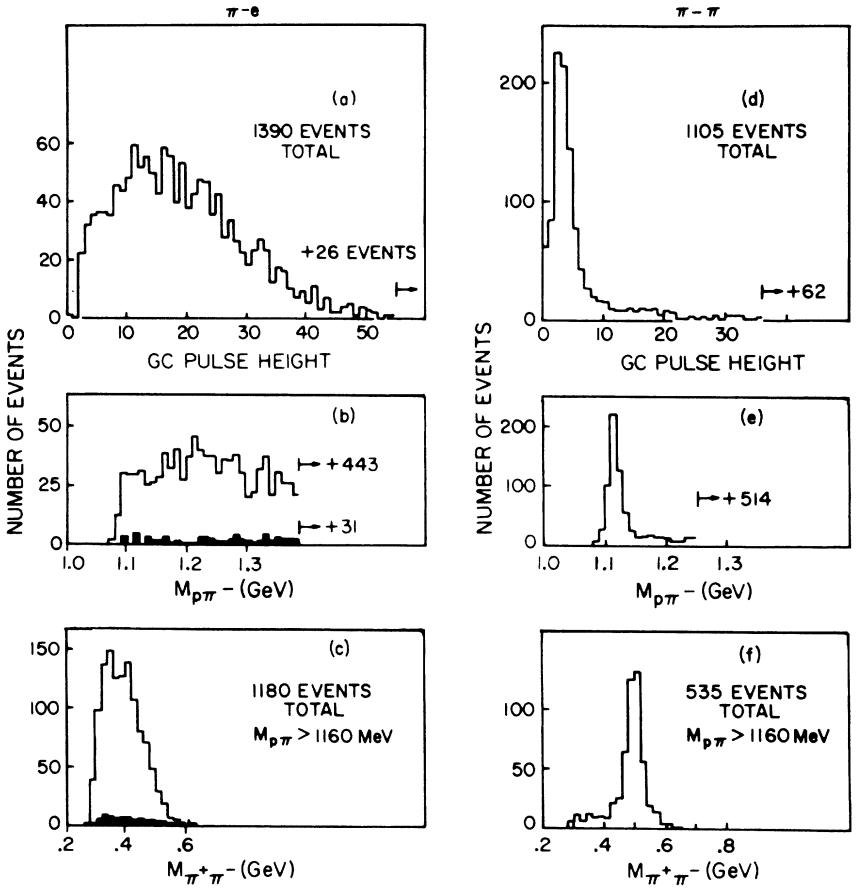


FIG. 2. Distributions in (*a*), (*d*) pulse height for the gas Čerenkov counter; (*b*), (*e*) invariant mass $M_{p\pi}$; and (*c*), (*f*) $M_{\pi\pi}$ for the $K_{e3}$ sample ($\pi e$) and $K_{\pi\pi}$ sample ($\pi\pi$). The latter sample was selected during the scan of the shower chambers as consisting of two nonshowering particles. The $\pi\pi$ sample shows a large peak at low GC pulse height, corresponding to triggering by noise and $\delta$ rays. This sample also shows large component of $\Lambda$ and $K \to \pi\pi$ decays. The shaded events have GC < 8 and decay time $\lesssim 2\tau_S$. No background is evident.

requiring a large rejection factor ($10^5$). This was accomplished by the combined use of the Cerenkov counter, the shower chambers, and the shower counters to distinguish electrons from protons and pions. An additional handle on this background is the invariant mass calculated from the measured momenta of the charged secondaries in observed events. The two-body backgrounds were low enough so that it was not necessary to remove events on that basis. By comparing the "$\pi\pi$ sample" (see Sec. III) with the data ("$\pi e$"), we were able to estimate the magnitude of these backgrounds.

The pulse-height distributions in the gas Čerenkov counter (GC) are shown for the $\pi e$ and $\pi\pi$ sample in Figs. (2a) and (2d). The effect of the triggering threshold bias can be seen in Fig. (2d). By comparison, the events in the $\pi e$ sample (2a) have many more events at large pulse height. The invariant mass distributions in the $\pi\pi$ sample [(2e) and (2f)] show peaks corresponding to $\Lambda^0$ and $K^0$ two-body decay. The $\pi e$ sample [(2b) and (2c)] shows no such effect. From these distributions, we see no evidence for significant background.

By investigating the invariant mass distributions as a function of cuts on the Čerenkov counter pulse height, we have determined the amount of such backgrounds in the $\pi e$ sample with good precision, and determined the efficiency of this procedure on actual background. We estimate that there are $7.8 \pm 10.0$ such background events. This is consistent with rejection factors of the shower chambers estimated independently, which give $8.0 \pm 4.0$ background events in the sample.

We emphasize that these background estimates are without any cuts in either Čerenkov counter pulse height or invariant mass. The background can be reduced even further in order to demonstrate insensitivity of our result to it. For example, by removing events with $p\pi^-$ invariant mass less than 1160 MeV or $\pi^+\pi^-$ invariant mass greater than 440 MeV, simultaneous with the gas counter pulse height less than 8, we reduce this background further by a factor of three.

The next potential source of background in Table I is the $e$-pair production. This comes from $\gamma$ rays converting in the production-decay region ($\gamma + Z \to e^+e^- + Z$) and from Dalitz decays of $\pi^0$ ($\pi^0 \to e^+e^-\gamma$) resulting from neutral $K$ and $\Lambda$ decays ($K_S \to \pi^0\pi^0$ and $\Lambda \to n\pi^0$). The shape of the $e^+e^-$ mass distribution (see Fig. 3) indicates that the $\gamma$-ray conversion background is less than 9 events. Studies of $\gamma$-ray conversion in 0.25 radiation lengths of lead placed in the production-decay region indicate that the mass cut $M_{e^+e^-} > 0.030$ GeV removes 97% of the conversion background, leaving less than 0.3 events.

The number of $e$ pairs from Dalitz decays of $\pi^0$ resulting from $K_S \to \pi^0\pi^0$ decays was determined by a Monte Carlo calculation. This calculation indicated that without the shower-chamber scan or the $M_{e^+e^-}$ cut there should be 880 such events in the $K_{e3}$ sample. The $e$-pair rejection of the shower-chamber scan was determined to be $(43 \pm 11)/1$ by scanning known $e$-pair events for "$\pi$-$e$" events. This would leave $20 \pm 5$ in the data sample. The $M_{e^+e^-}$ cut at 0.030 GeV reduces this background to $12 \pm 3$ events. Moving the cut $M_{e^+e^-} > 0.060$ GeV further reduces it by a factor of 5. This was done in one of the fits to check the sensitivity of $X$ to this background.

The $\Lambda \to pe\nu$ background was estimated by comparing the $p$-$e$ (assumes the pion is a proton) mass of the $\pi^+e^-$ events with that of the $\pi^-e^+$ events. The excess of events in the region $M_{pe} < 1.115$ GeV for the $\pi^+e^-$ events was assumed to be caused by $\Lambda$-$\beta$ decay. This leads to an estimate of $16 \pm 8$ background events before the mass cut at 1.115 GeV. This cut removes all the background except for a very small amount resulting from spill-over due to mass resolution. The cut was made on both the $\pi^+e^-$ and the $\pi^-e^+$ events in order to preserve charge symmetry in the data.

$\bar{K}^0$ production in the target might arise from $K^0$-$\bar{K}^0$ pair production and from charge exchange of $K^-$'s in the $\pi^-$ beam. Bubble-chamber data[10] indicates that $\bar{K}^0$ production is only 10% as frequent as $K^0$ production at the $\pi^-$ momentum of this experiment. Because of the lower momenta and

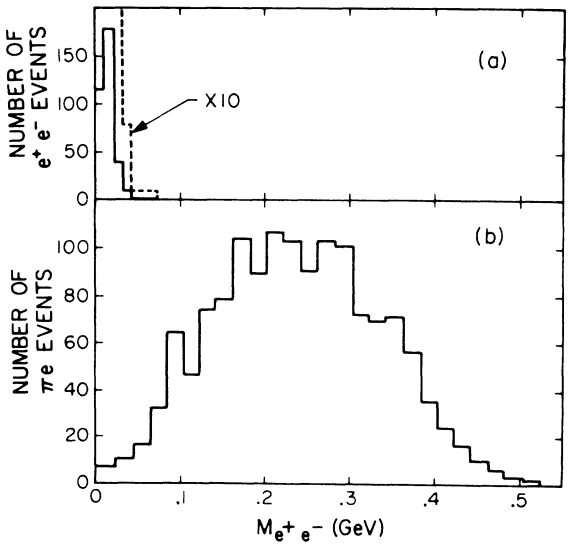


FIG. 3. Comparison of (a) the $e^+e^-$ invariant-mass distribution of a sample of $\gamma$ rays converted in lead, and (b) the $e^+e^-$ mass distribution for the $\pi e$ sample. The two samples were scanned and measured identically.

the wider angular distribution of the $\overline{K}^0$'s, the acceptance was calculated to be smaller by more than a factor of 10. Therefore the contamination from $K\overline{K}$ production is less than 1%. The $K^-$ beam contamination was determined to be $0.1\% \pm 0.05\%$ from time-of-flight measurements in conjuction with an $SF_6$ beam Čerenkov counter. Because the charge-exchange cross section for $K^-$'s is 5 times greater than that for $K^0$ production with $\pi^-$'s, the $\overline{K}^0$ contamination from this source is 0.5%. These estimates are consistent with fits to the data in which the $\overline{K}^0$ contamination was a free parameter. The contamination parameter so determined was $(0.6 \pm 1.9)\%$.

The total background, in the sample of 1137 events, from the above sources excluding $K\overline{K}^0$ pair production is $25 \pm 12$ events. The $K\overline{K}$ pair production is estimated to contribute less than 11 events.

### $K \to \pi^+\pi^-\pi^0$ Remnant Backgrounds

The discussion of backgrounds in this decay mode is divided into those with a flat time distribution and those with an exponential distribution. The latter type is a more serious source of bias. Both types of backgrounds are summarized in Table II.

The principal sources of background were $K_S \to \pi^+\pi^-$ and $\Lambda \to p\pi$ with one or more associated $\gamma$ rays. In the $K_S \to \pi^+\pi^-$ case the $\gamma$ ray might have come from $\Lambda \to n\pi^0$ followed by $\pi^0 \to 2\gamma$. In the $\Lambda \to p\pi$ background the $\gamma$ ray might have come from $K_S \to \pi^0\pi^0$ followed by $2\pi^0 \to 4\gamma$. It was also possible for the $\gamma$ ray to come from the $\pi^0$ production in the target, although the $\gamma$ rays from this source had a high probability of converting in the target, thus vetoing the event.

The $\Lambda \to p^+\pi^-$ background was removed by cutting out events with a $p^+$-$\pi^-$ (assumes the + track is a proton and the negative one is a $\pi^-$) invariant mass less than 1.2 GeV [see Fig. 4(a)]. The details of the resolution on individual measurements were studied using calibration run data [see Fig. 4(b)]. This study allows an estimate of $(-1.5 \pm 5)$ $\Lambda \to p\pi$ events in the data with $M_\Lambda > 1.2$ GeV. It should be

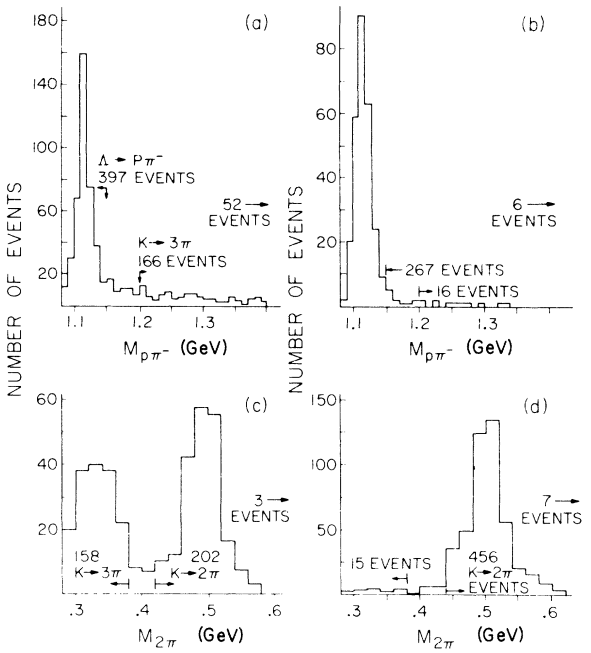


FIG. 4. Invariant mass distributions $M_{p\pi}$ [(a), (b)] and $M_{2\pi}$ [(c), (d)]. (a), (c) are the $\pi^+\pi^-\pi^0$ data, while (b), (d) are the calibration $K \to \pi^+\pi^-$ data. The $M_{p\pi}$ distributions contain data with $M_{2\pi} < 0.4$ GeV to remove the $K \to 2\pi$ component. The $M_{2\pi}$ distributions have $M_{p\pi} > 1.2$ GeV to remove the $\Lambda \to p\pi$ component. The $K \to \pi^+\pi^-\pi^0$ signal is clearly evident in (c) with $M_{2\pi} < 0.38$ GeV.

TABLE II. Background in the $K \to 3\pi$ sample (148 events).

| Background | Time distribution | Number of events in data sample |
|---|---|---|
| $\Lambda \to p^+\pi^-$ | Exponential | $-1.5 \pm 5$ |
| $K_S \to \pi^+\pi^-$ | Exponential | $4 \pm 3$ |
| $K_L \to \pi\mu\nu$ | Flat | $2 \pm 1.5$ |
| $K_S \to \pi^+\pi^-\gamma$ | Exponential | $3 \pm 2$ |
| $\pi^0 \to 2\gamma \to e^+e^-\gamma$ | Flat or exponential | <3 |
| Neutron stars | Flat | $4 \pm 2$ |
| $\overline{K}^0 \to \pi^+\pi^-\pi^0$ | Flat | <2 |
| | Total exponential | $5.5 \pm 6$ |
| | Total flat | $6 \pm 5$ |

remarked that this cut at 1.2 GeV removes ~30% of the $K \to \pi^+\pi^-\pi^0$ events and that they are removed in a charge-asymmetric way. The effect of this induced asymmetry on the time distribution is at the 1% level (an interference effect might occur through the transition to the $I=2$ $\pi\pi\pi$ state which is suppressed by both the $\Delta I = \frac{1}{2}$ rule and a centrifugal barrier).

Figure 4(d) shows the invariant $\pi^+\pi^-$ mass for the calibration run data ($K_S \to \pi^+\pi^-$) and Fig. 4(c) shows this for the $K \to 3\pi$ data. The $K \to 3\pi$ signal lies at $M_{\pi^+\pi^-} < 0.38$ GeV in the latter distribution. Note that in the $\pi^+\pi^-$ data there are 15 events in the tail with $M_{\pi^+\pi^-} < 0.38$ GeV. This number is consistent with the 3-body decays expected. An upper limit on the background in the $K \to 3\pi$ sample was obtained by assuming that these 15 events were all background. An investigation of their time distribution then indicates that there are about $(4 \pm 3)$ $K_S \to \pi^+\pi^-$ events in the $3\pi$ data with $M_{\pi^+\pi^-} < 0.38$ GeV, and about $(2 \pm 1.5)$ $K_L^0 \to \pi\mu\nu$ events in the data.

To estimate the background from $K_S^0 \to \pi^+\pi^-\gamma$, we note that this decay takes place at early times, and preferentially produces events with invariant mass $M_{\pi\pi} > 0.38$ GeV. By comparing the mass distribution for events both at early times and in the region $0.38 < M_{\pi\pi} < 0.42$ GeV, between calibration runs (no additional $\gamma$) and the data shown in Fig. 4(c), we estimate that the number of $\pi\pi\gamma$ events with $M_{\pi\pi} < 0.38$ GeV is $3 \pm 2$.

The $\pi^0 \to 2\gamma \to e^+e^-\gamma$ background was removed by the Čerenkov counter. As a check, we find there are only three events with $M_{e^+e^-} < 30$ MeV, so we can put an upper limit of three events on this background.

The multiprong neutron stars were retained during the scan of the production-decay region. Only two stars with three or more prongs were found in the final data sample. Assuming that the 2-prong stars are of comparable number we estimate the number of stars to be $4 \pm 2$. The position distribution of these events is flat.

From the analysis at the end of the section on $K_{e3}$ backgrounds, the $\overline{K}^0$ contamination is less than 1.5%, corresponding to 2 events of the form $\overline{K}^0 \to \pi^+\pi^-\pi^0$. The distribution of these events is flat if $CP$ is conserved. Otherwise it cancels the interference term in the $K^0 \to \pi^+\pi^-\pi^0$ distribution.

To summarize this background discussion, there are $5.5 \pm 6$ background events resulting from $K_S$ and $\Lambda$ decays. This is consistent with a fit in which a background term was included. The fit gave the short-lived background term as $0^{+8}_{-0}$ events. In addition, there are $6 \pm 5$ background events with a flat spatial distribution. These are not expected to affect the fit to $W$ significantly.

## V. MONTE CARLO CALCULATIONS

In order to calculate the efficiency function for $K \to \pi e\nu$ and $K \to \pi^+\pi^-\pi^0$ the momentum and angular distributions of the $K^0$'s emerging from the targets had to be determined. This was done by isolating a sample of $K^0 \to \pi^+\pi^-$ events from the calibration runs, and determining the momentum and angular distribution of the accepted events. A Monte Carlo calculation of the apparatus acceptance at a number of $K^0$ production angles and momenta was then used to unfold the $K^0$ production distributions from the distributions of the accepted calibration run events. The resulting distribution in angle and momenta of $K^0$'s produced in brass by 2.85-GeV/$c$ $\pi^-$ are shown in Fig. 5. The observed distributions for $K^0 \to 2\pi$ data are shown in Figs. 6 and 7 as data points. The predicted distributions, using Fig. 5 as input, and $K \to 2\pi$ decay and acceptance folded in, as well as measurement errors, are shown as histograms. Figure 7 is the longitudinal position distribution of the $K \to 2\pi$ decays. Transverse position distributions at various apertures in the apparatus for charged secondaries also agreed well with those of the Monte Carlo events.

$$A_{\pi e \nu}(L)$$

The $K \to \pi e\nu$ acceptance function, $A_{\pi e\nu}(L)$, was subsequently determined as a function of decay

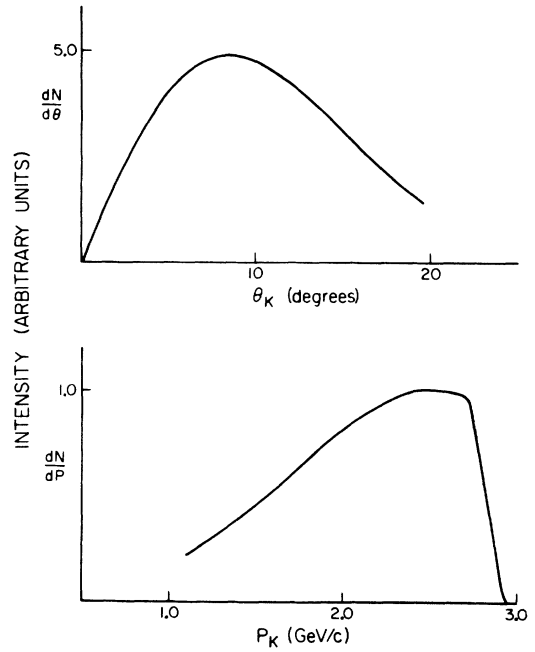


FIG. 5. The angular and momentum distributions of forward $K^0$'s produced in brass by 2.85-GeV/$c$ negative pions, as determined by analysis of $K \to 2\pi$ decays.

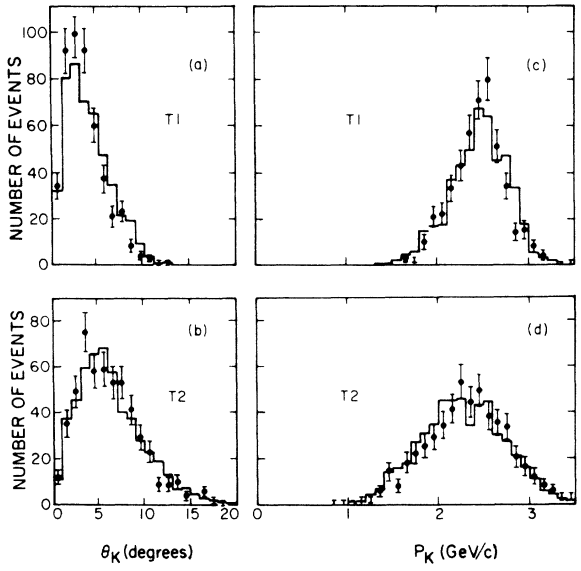


FIG. 6. Comparison of the angular and momentum distributions for the $K \to \pi^+\pi^-$ data (points) and the Monte Carlo events (histogram). The comparison is done separately for targets $T1$ and $T2$.

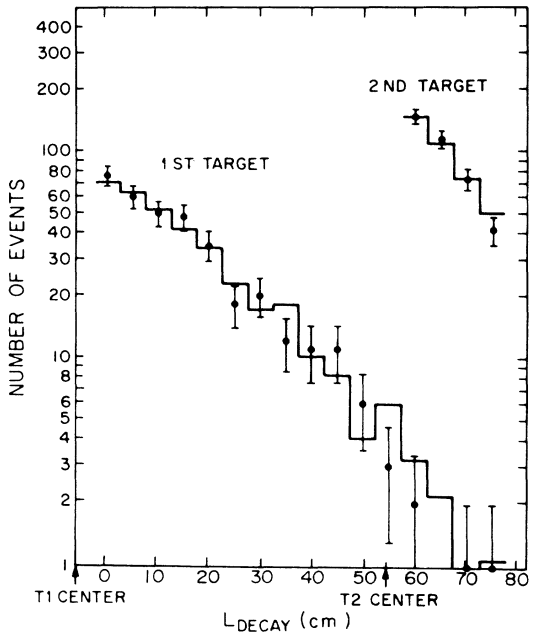


FIG. 7. Comparison of the decay length distributions for $K \to \pi^+\pi^-$ data (points) and the Monte Carlo events (histograms).

length by generating $K \to \pi e \nu$ decays at fixed longitudinal positions using the $K^0$ angular and momentum distributions previously discussed. Events were generated at six positions 5 in. apart for $T1$ and at two positions 5 in. apart for $T2$. The acceptance at these positions was then fitted to a quadratic form (in $L$, the longitudinal position) for $T1$ and a linear form for $T2$.

Besides the geometric constraints imposed by the apparatus design, the Monte Carlo calculation included the electron energy-dependent bias (see Fig. 8) caused by the shower-counter pulse-height requirement. It also included the mass cuts $M_{e^+e^-} > 0.030$ GeV and $M_{pe} > 1.115$ GeV. As a check on this calculation, various distributions of the accepted Monte Carlo events were compared with those of the data. The distributions of electron momenta, pion momenta, pion+electron momenta [see Fig. 9(a)], electron-pion invariant mass, and track position distributions at various apertures in general agreed. To further check the gas counter the average pulse height as a function of decay position was studied. This study indicated that the variation in efficiency of the gas counter over the range of decay length ($L$) was less than 1.2%.

The data were taken at two magnetic field settings (2.0 and 2.8 kG). Slightly different efficiency functions were calculated for use with the data, one for each field setting. Figure 10(a) shows the weighted average of these two efficiency functions.

$A_{3\pi}(L)$

The momentum and angular distributions of the $K^0$'s determined from the calibration data ($K \to \pi^+\pi^-$) were used in a Monte Carlo calculation to determine the acceptance, $A_{3\pi}(L)$, for $K \to \pi^+\pi^-\pi^0$ at four decay lengths 10 in. apart. The acceptances at these points were then fitted to a straight line. This was done separately for the

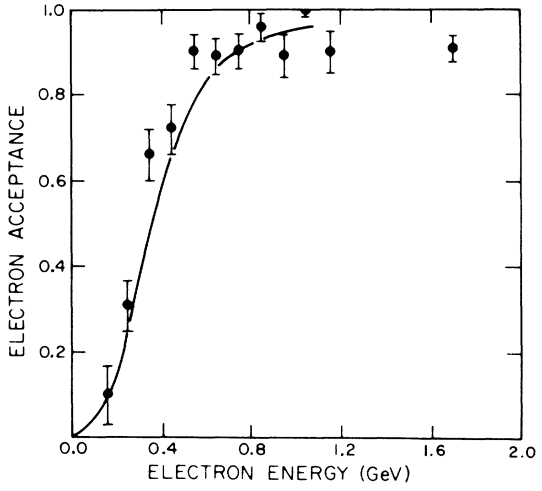


FIG. 8. The data points are the measured electron acceptance of the shower counters with a 1.7 minimum-ionizing bias. The solid curve is the calculated acceptance with a 2.0 minimum-ionizing bias.

two magnetic field settings. Figure 11(a) shows the weighted average of the two calculations.

The Monte Carlo calculation included the dependence of the decay matrix element on the kinetic energy of the $\pi^0$ in the center-of-mass system:

$$1 + 2SM_K(2T_{\pi 0} - T_{\max})/M_\pi{}^2,$$

where $T_{\pi 0}$ is the center-of-mass $\pi^0$ kinetic energy; $T_{\max}$ is 0.053 GeV; and $M_K$ and $M_\pi$ are the kaon and pion masses. The parameter $S$ was taken to be $-0.30$ on the basis of experiments on $K_L \to \pi^+\pi^-\pi^0$.[11] As a check, we analyzed the $K \to 3\pi$ data to determine $S$ independently. Figure 12 shows the Dalitz plot density versus $T_{\pi 0}$. We find $S = -0.28 \pm 0.05$.

The Monte Carlo calculation also included the effects of the shower counter threshold (2 times minimum ionizing) and the computer scan on the $\gamma$ ray acceptance. This acceptance was calculated using shower calculations[12] in this energy region. These calculations agree well into the efficiency for electron acceptance versus energy measured from the $K_{e3}$ sample (see Fig. 8).

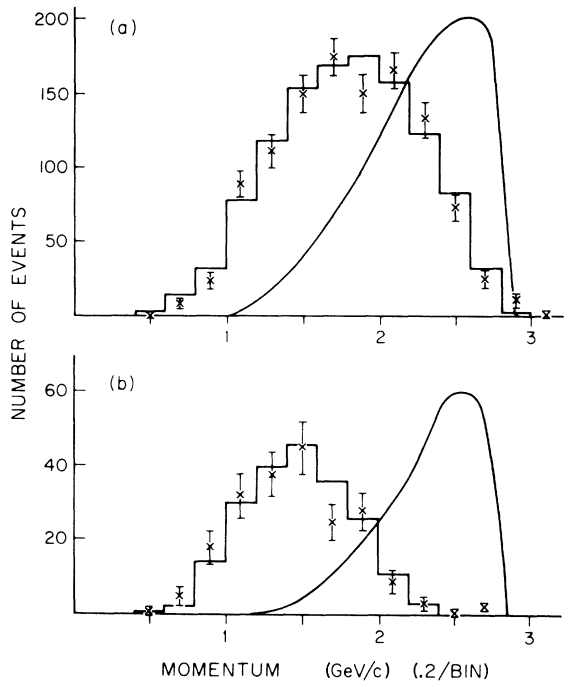


FIG. 9. (a) Comparison of the $\pi e$ total momentum for the $K_{e3}$ data (data points) with the accepted Monte Carlo events (histograms). The solid curve is the total $K^0$ momentum of the accepted Monte Carlo events. (b) Comparison of the $\pi^+\pi^-$ total momentum for the $K_{\pi 3}$ data (data points) with the accepted Monte Carlo events (histograms). The solid curve is the total $K^0$ momentum of the accepted Monte Carlo events.

When all the above effects were taken into account the distributions of the Monte Carlo events were compared with the data events. Typical distributions which were compared were the momentum distributions of the pions, the distributions of the sum of the pion momenta [see Fig. 9(b)], the invariant-mass distributions, the pion opening-angle distribution, the track-position distributions at the various counter apertures, and the $\gamma$-ray-position distributions in the shower counters. There was generally agreement between the Monte Carlo-generated distributions and the data.

## VI. LIKELIHOOD FITS

In this experiment, individual events are not reconstructed kinematically. This means that the $K^0$ momentum is not determined on an individual basis. However, the decay position is measured for each event. The distribution in decay positions, $L$, is given by

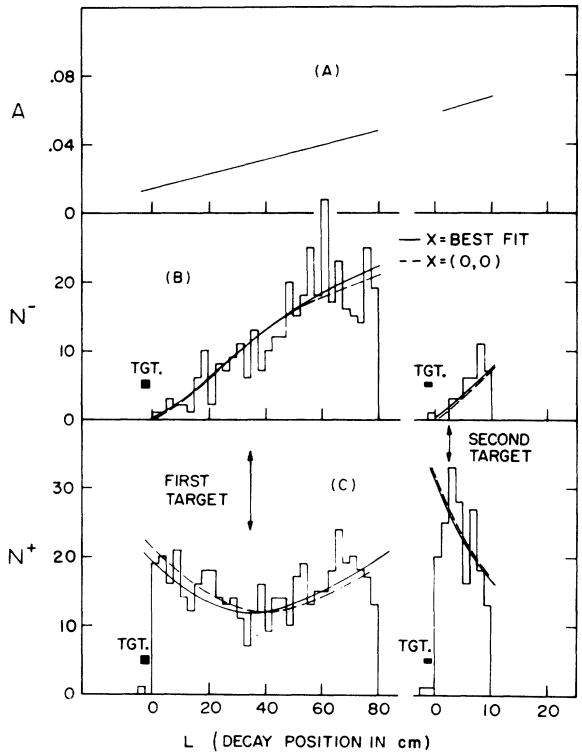


FIG. 10. (a) Efficiency ($A_{\pi e \nu}$) for $K_{e3}$ detection as a function of the decay position for both targets, (b) position distribution for the $\pi^+e^-\nu$ events, (c) position distribution for the $\pi^-e^+\nu$ events. Curves calculated from $F^+$ and $F^-$ are shown for three values of $X$. Distance is measured from the beginning of the fiducial volume. The target centers are at $-1.5$ in.

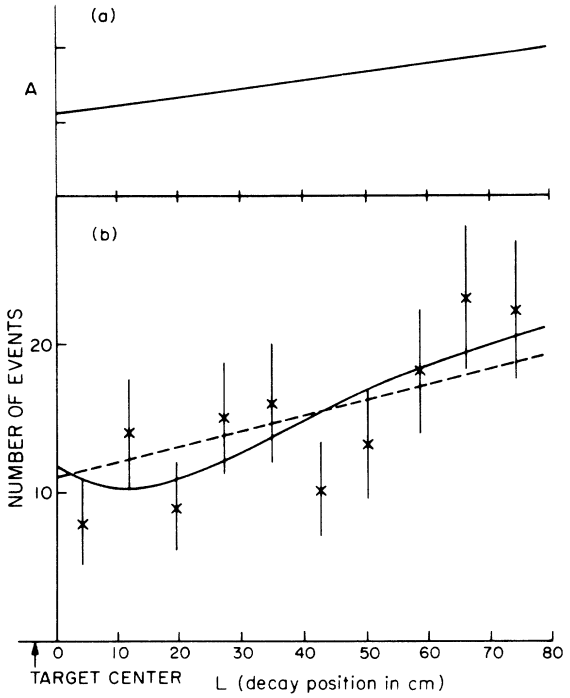


FIG. 11. (a) The detection efficiency ($A_{3\pi}$) and (b) the data sample position distribution for $K \to \pi^+\pi^-\pi^0$ events. The solid curve is the calculated distribution for our best fit to $W$ and the dashed line corresponds to $W=0$.

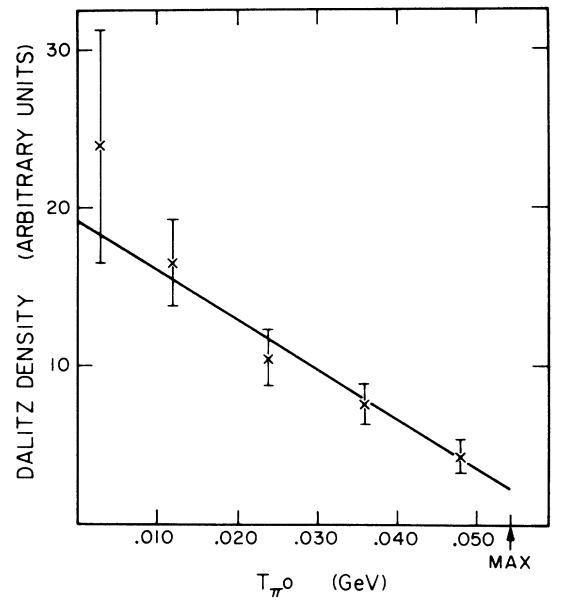


FIG. 12. The Dalitz plot density of the $K \to 3\pi$ data (148 events). $T_{\pi^0}$ is the c.m. $\pi^0$ kinetic energy. The data bins have been corrected for mass resolution.

$$G(L) = \frac{dN}{dL} = \int F\left(\frac{mL}{pc}\right) \frac{m}{pc}\, \epsilon(p, L)\rho(p)\, dp\,, \qquad (7a)$$

where $F(t)$ is one of the distributions (4) or (5);

$\rho(p)\,dp$ is the number of $K^0$ of momentum $p$ produced in the target,

$\epsilon(p, L)$ is the probability for the apparatus to accept a $K^0$ decay of momentum $p$ at position $L$,

$c$ is velocity of light.

Expanding the time distribution in a Taylor series,

$$F\left(\frac{mL}{pc}\right) = F\left(\frac{mL}{p_0c}\right) - F'\left(\frac{mL}{p_0c}\right)\frac{mL}{p_0^2c}(p-p_0) + \frac{1}{2}\left[\left(\frac{mL}{p_0^2c}\right)^2 F'' + \frac{2mL}{p_0^3c}F'\right](p-p_0)^2 + \cdots,$$

so that $G(L) = G_1(L) + G_2(L) + \cdots$ corresponding to the various terms in the series. Then

$$G_2(L) = -\frac{m^2L}{p_0^2c^2}F' \int \rho(p)\epsilon(p, L)\frac{p-p_0}{p}\, dp\,.$$

By choosing

$$p_0(L) = \frac{\int \rho(p)\epsilon(p, L)\, dp}{\int \rho(p)\epsilon(p, L)\, dp/p}\,,$$

this term disappears, and the first-order term becomes

$$G_1(L) = \frac{m}{p_0c} F\left(\frac{mL}{p_0c}\right) A(L)\,, \qquad (7b)$$

where $A(L) = \int \rho(p)\epsilon(p, L)\, dp$ is the acceptance function for decays of the specific type. This function was calculated with the Monte Carlo calculation described in Sec. V. The same calculation gave $p_0$. It was found, for all decay types, that $p_0$ was independent of decay position, $L$. A straightforward calculation yields for the relative contribution of the next-order term

$$G_3(L) = \frac{1}{2}\left(\frac{\sigma_p}{p_0}\right)^2 (F''t^2 + 2F't)A(L)\,,$$

where $t = mL/p_0c\tau_S$ is the proper time for decay in units of the $K_S^0$ lifetime and $\sigma_p$ is the standard deviation of the momentum distribution for accepted $K^0$ decays. The factor $(F''t^2 + 2F't)$ is zero at $t=0$ and $t=\infty$, and has absolute value less than one for the distributions (4) or (5) in the region of interest. Using the mean momentum for accepted events (typically $p_0 = 2.25$ GeV/$c$) and the standard

deviation (typically $\sigma_p = 0.39$ GeV/$c$), we find $G_3(L) < 0.015A(L)$. For the $K_{e3}$ experiment, this third-order term corresponds to less than about 1.5 events per $K_S^0$ lifetime. This is negligible compared to the statistical accuracy of the data (~200 events per lifetime). A calculation of the exact expression, Eq. (7a), shows that

$$|G(L) - [G_1(L) + G_3(L)]| \ll G_3(L),$$

justifying neglect of higher-order terms.

In order to determine the best values of the fitted parameters, a maximum-likelihood search was performed using the position distribution $G(L) = G_1(L) + G_3(L)$, according to Eqs. (7b) and (7c). It is the results of these fits which are reported here. As a check, we determined the best fit using only $G_1(L)$. As expected, these results in general differed from those including the third-order term by less than 10% of a standard deviation.

$$K^0 \to \pi^\pm e^\mp \nu$$

Figures 10(b) and 10(c) show the position distributions for the 1079 accepted $K_{e3}$ events. Assuming *CPT* invariance ($X_+ = X_-^* = X$) (Ref. 13) and using Ref. 14 for the values of the parameters $\tau_S$, $\tau_L$, and $\Delta M$ ($\Delta M = |\Delta M|$) the best fit of our data to Eq. (4) gives

$$\mathrm{Re}X = -0.070 \pm 0.036,$$

$$\mathrm{Im}X = +0.107^{+0.092}_{-0.075}.$$

Figure 13 shows the likelihood contours. The $X = 0$ point has a probability of 25% relative to the best value, and is consistent with the data.

Table III shows the results from other likelihood fits made with a variety of assumptions. In particular, the data are consistent with *CPT* invariance, and with the accepted value of the $K_L^0$-$K_S^0$ mass difference.

The data are also consistent with negligible

TABLE III. Fits to the $K_{e3}$ sample.

| Run condition | Number of events | $\mathrm{Re}X_+$ | $\mathrm{Im}X_+$ | Third parameter |
|---|---|---|---|---|
| Final result | 1079 | $-0.070 \pm 0.036$ | $+0.107^{+0.092}_{-0.075}$ | None |
| Positive electrons only | 672 | $-0.077 \pm 0.072$ | $+0.016^{+0.160}_{-0.190}$ | None |
| Negative electrons only ($\mathrm{Im}X_- = -\mathrm{Im}X_+$) | 407 | $-0.045^{+0.054}_{-0.068}$ | $+0.168^{+0.084}_{-0.102}$ | None |
| $\Delta m$ is a free parameter | 1079 | $-0.081^{+0.034}_{-0.036}$ | $+0.101^{+0.094}_{-0.088}$ | $\Delta m \tau_S = 0.424^{+0.052}_{-0.048}$ |
| $\bar{K}$ contaminations is a free parameter ($N_{\bar{K}} = 1 - N_K$) | 1079 | $-0.056^{+0.036}_{-0.038}$ | $+0.116^{+0.082}_{-0.080}$ | $N_{\bar{K}} = 0.006^{+0.019}_{-0.006}$ |
| Reduce $K^0 \to \pi^+\pi^-$ and $\Lambda^0 \to p\pi^-$ by a factor of 3 | 1031 | $-0.065^{+0.034}_{-0.038}$ | $+0.092^{+0.104}_{-0.068}$ | None |
| Reduce Dalitz background by a factor of 4.8 | 1066 | $-0.070^{+0.034}_{-0.036}$ | $+0.108^{+0.096}_{-0.072}$ | None |
| Fix Re$X$ at 0 | 1079 | ... | $+0.02^{+0.058}_{-0.060}$ | None |
| Fix Im$X$ at 0 | 1079 | $-0.036^{+0.036}_{-0.044}$ | ... | None |
| Increase $P_0$ by 0.05 GeV/$c$ | 1079 | $-0.078^{+0.034}_{-0.036}$ | $+0.112^{+0.080}_{-0.080}$ | None |
| Decrease $P_0$ by 0.05 GeV/$c$ | 1079 | $-0.061^{+0.034}_{-0.036}$ | $+0.107^{+0.086}_{-0.010}$ | None |
| Move average production point upstream by 0.25 in. | 1079 | $-0.049^{+0.034}_{-0.036}$ | $+0.104^{+0.092}_{-0.074}$ | None |
| Move average production point downstream by 0.25 in. | 1079 | $-0.085^{+0.032}_{-0.038}$ | $+0.096^{+0.092}_{-0.078}$ | None |
| Lower Monte Carlo $P_0$ by 0.10 GeV/$c$ | 1079 | $-0.042^{+0.034}_{-0.036}$ | $+0.072^{+0.110}_{-0.070}$ | None |
| Asymmetry only | 1079 | $-0.068^{+0.036}_{-0.038}$ | $+0.181^{+0.110}_{-0.160}$ | None |
| Sum only | 1079 | $-0.076^{+0.086}_{-0.118}$ | $+0.100^{+0.092}_{-0.112}$ | None |

backgrounds, as determined independently (see Sec. IV), and are consistent with the absence of experimentally induced biases. In particular, the result obtained from the asymmetry alone is in good agreement with the result obtained from the sum of positives and negatives. [Because Eq. (7b) is a good approximation to (7a), the asymmetry is essentially independent of efficiency.]

Table IV (data taken from Refs. 15–25) gives a compilation of experimental values for the $\Delta S/\Delta Q$-violating parameter, $X$. The world average, $\mathrm{Re}X = +0.016 \pm 0.021$, $\mathrm{Im}X = -0.013 \pm 0.018$, is consistent with zero.

$$K \to \pi^+\pi^-\pi^0$$

The position distribution of the 148 accepted $K \to \pi^+\pi^-\pi^0$ decays was fitted to Eqs. (5) and (7). The best value for $W$ was found to be

$$\mathrm{Re}W = -0.05 \pm 0.17,$$

$$\mathrm{Im}W = +0.39^{+0.35}_{-0.37}.$$

The theoretical position distribution (solid curve) with this value of $W$ is compared with the data in Fig. 11(b). The dashed line corresponds to the distribution for $W = 0$ and has a $\chi^2$ of 9.5 for 9 degrees of freedom. The likelihood contours for the fit to $W$ are shown in Fig. 14.

Table V shows the likelihood fits which are obtained by varying the efficiency function, the mass

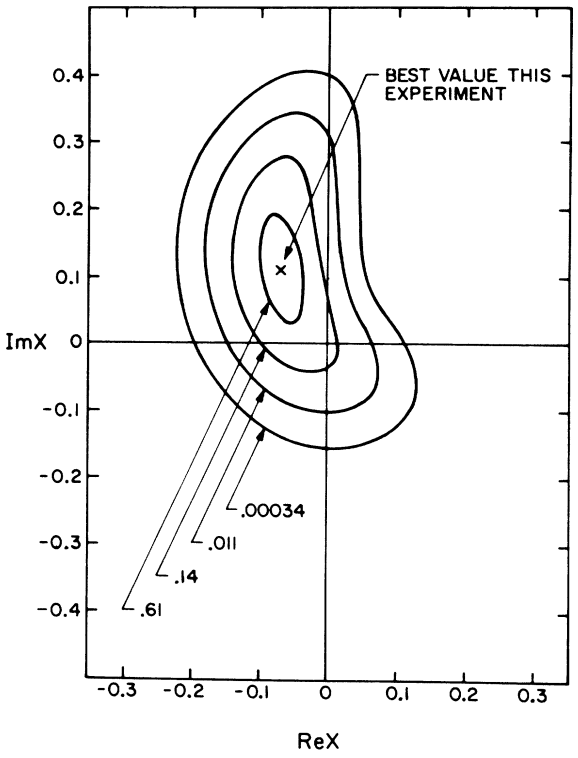


FIG. 13. The best value for $X$ from this experiment ($K_{e3}$ data). Also shown are the contours corresponding to the 1-, 2-, 3-, and 4-standard-deviation limits.

TABLE IV. $K_{e3}$ compilation.

| Group | Method | Number of $K \to \pi l \nu$ events | Re$X$ | Im$X$ | Ref. |
|---|---|---|---|---|---|
| Paris (1965) | Freon/Prop. B. C., $K^+N \to K^0p$ | 315 | $0.035^{+0.11}_{-0.13}$ | $-0.21^{+0.11}_{-0.15}$ | 15 |
| Padua (1965) | Heavy liquid B. C., $K^+N \to K^0$ | 152 | $0.06^{+0.18}_{-0.44}$ | $-0.44^{+0.32}_{-0.19}$ | 16 |
| Columbia/Rutgers (1965) | $H_2$ B. C., $\bar{p}-p$ | 109 | $0.08^{+0.16}_{-0.28}$ | $0.24^{+0.40}_{-0.30}$ | 17 |
| Penn. (1967) | Sp. chamber, $\pi^-p \to K^0\Lambda$ | 116 | $0.17^{+0.16}_{-0.35}$ | $0.00 \pm 0.25$ | 18 |
| Brookhaven/Carnegie (1970) | $D_2$ B. C., $K^+N \to K^0p$ | 215 | $0.12 \pm 0.09$ | $-0.08 \pm 0.07$ | 19 |
| Berkeley (1971) | $D_2$ B. C., $K^-p \to \bar{K}^0N$ | 252 | $0.25^{+0.07}_{-0.09}$ | $0.00 \pm 0.08$ | 20 |
| CERN/Paris (1968) | $H_2$ B. C., $\bar{p}-p$ | 121 | $0.09^{+0.13}_{-0.11}$ | $0.22^{+0.29}_{-0.37}$ | 21 |
| San Diego (1969) | Sp. chamber, $K^+\mathrm{Cu} \to K^0$ | 686 | $0.09^{+0.14}_{-0.16}$ | $-0.11^{+0.10}_{-0.11}$ | 22 |
| Caltech (1971-72) | Sp. chamber, $\pi^-\mathrm{Cu} \to K^0$ | 1079 | $-0.070 \pm 0.036$ | $0.107^{+0.092}_{-0.074}$ | 23 This exp. |
| Illinois/Northeastern (1971) | $\pi^-\mathrm{C} \to K^0\Lambda$ | 342 | $-0.13 \pm 0.11$ | $-0.04 \pm 0.16$ | 24 |
| CERN/Orsay/Vienna (1971) | $K^+p \to K^0p\pi^+$ | 5800 | $0.05^{+0.021}_{-0.035}$ | $-0.01 \pm 0.02$ | 25 |
| Average | | 9187 | $0.016 \pm 0.021$ | $-0.013 \pm 0.018$ | |
| | | | $\chi^2 = 17.3$ with 10 d.f. | $\chi^2 = 10.7$ with 10 d.f. | |

cuts, and the input parameters to Eq. (7). The efficiency function was changed by twice the expected error from statistical and systematic effects in the Monte Carlo calculation. The $2\pi$ mass cut was moved to a place where the background from $K_S$ decays would be doubled. These variations changed $W$ by a fraction of a standard deviation. The changes in $W$ from movement of the $p\pi$ mass cut are consistent with the change in the statistics.

Table VI (data taken from Refs. 26–34) shows a compilation of experimental values for $W$. The data are quite consistent and give an over-all average that is consistent with zero: $\mathrm{Re}W = +0.10 \pm 0.09$; $\mathrm{Im}W = +0.24 \pm 0.16$. However, this compilation does not completely rule out a sizable $CP$ violation as discussed in Sec. I.

## VII. CONCLUSIONS

Our best fit to the final sample of 1079 $K_{e3}$ events gives

$$\mathrm{Re}X = -0.070 \pm 0.036,$$

$$\mathrm{Im}X = 0.107^{+0.092}_{-0.074}.$$

The time distributions are consistent with $CPT$ invariance $[(X_+ - X_-^*) = 0]$. The errors from systematic effects and backgrounds are small compared

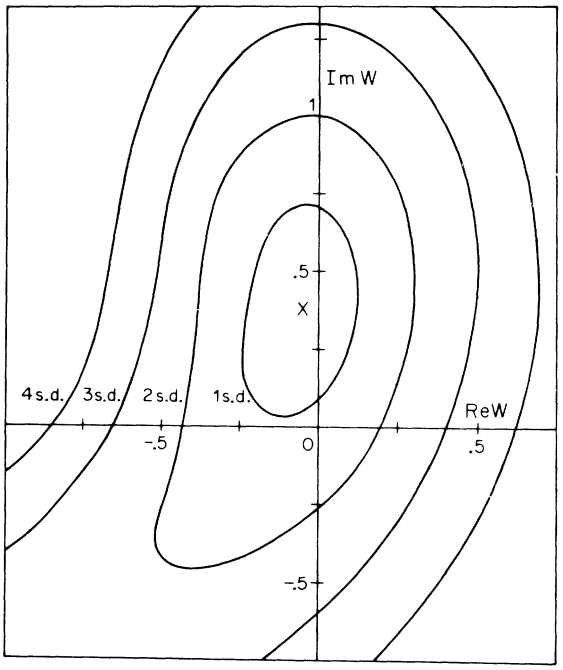


FIG. 14. The best value for $W$ from this experiment ($K \to 3\pi$ data). The 1-, 2-, 3-, and 4-standard-deviation contours are shown. The 3- and 4-standard-deviation contours do not close in the lower left-hand quadrant for $|W| < 1.5$.

TABLE V. Fits to the $K \to 3\pi$ sample.

| Run conditions | Number of events | Re$W$ | Im$W$ |
|---|---|---|---|
| Final result | | | |
| $M_K < 0.38$ GeV, $M_\Lambda > 1.2$ GeV | 148 | $-0.05 \pm 0.17$ | $+0.39^{+0.35}_{-0.37}$ |
| $M_K < 0.36$ GeV, $M_\Lambda > 1.2$ GeV | 129 | $-0.01^{+0.20}_{-0.18}$ | $+0.25^{+0.4}_{-0.35}$ |
| $M_K < 0.42$ GeV, $M_\Lambda > 1.2$ GeV | 162 | $+0.08^{+0.19}_{-0.16}$ | $+0.30^{+0.35}_{-0.35}$ |
| $M_K < 0.38$ GeV, $M_\Lambda > 1.15$ GeV | 170 | $+0.04^{+0.17}_{-0.16}$ | $+0.43^{+0.37}_{-0.37}$ |
| $M_K < 0.38$ GeV, $M_\Lambda > 1.25$ GeV | 116 | $-0.02^{+0.21}_{-0.21}$ | $+0.15^{+0.35}_{-0.45}$ |
| $M_K < 0.38$ GeV, $M_\Lambda > 1.3$ GeV | 85 | $-0.01^{+0.23}_{-0.23}$ | $+0.53^{+0.40}_{-0.45}$ |
| Increase $\left(\frac{\text{efficiency slope}}{\text{average efficiency}}\right)$ by 30% | 148 | $-0.01^{+0.2}_{-0.17}$ | $+0.30^{+0.35}_{-0.37}$ |
| Decrease $\left(\frac{\text{efficiency slope}}{\text{average efficiency}}\right)$ by 40% | 148 | $-0.17^{+0.15}_{-0.17}$ | $+0.50^{+0.30}_{-0.30}$ |
| Increase $p_0$ by 0.1 GeV/$c$ | 148 | $-0.06^{+0.2}_{-0.16}$ | $+0.39^{+0.33}_{-0.34}$ |
| Decrease $p_0$ by 0.1 GeV/$c$ | 148 | $-0.04^{+0.16}_{-0.18}$ | $+0.39^{+0.33}_{-0.34}$ |
| Move average production point upstream 1.27 cm | 148 | $-0.04^{+0.19}_{-0.19}$ | $+0.39^{+0.35}_{-0.35}$ |
| Move average production point downstream 1.27 cm | 148 | $-0.09^{+0.18}_{-0.13}$ | $+0.39^{+0.3}_{-0.37}$ |

TABLE VI. $K \to 3\pi$ compilation.

| Method | Number of $K \to 3\pi$ events | Re$W$ | Im$W$ | Ref. |
|---|---|---|---|---|
| B. C., $K^+ d \to K^0 pp$ | 99 | $0.47 \pm 0.20$ | $-0.10^{+0.37}_{-0.32}$ | 26 |
| B. C., $K^- p \to \bar{K}^0 n$ | 50 | $2.75^{+0.65}_{-0.60}$ Re$W = 0$ at 2 s.d. | $+0.5^{+0.7}_{-0.55}$ | 27 |
| Heavy liquid B. C., $K^+ n \to K^0$ | 190 | | $+0.34^{+0.19}_{-0.58}$ Assumes Re$W = 0$ | 28 |
| Compilation of results of Refs. 29 and 30 by Ref. 30 | 71 | $0.05 \pm 0.30$ | $-0.15 \pm 0.45$ | 29, 30 |
| B. C., $K^+ p \to K^0 + p + \pi^+$ | 98 | $0.01^{+0.22}_{-0.20}$ | $+0.33^{+0.42}_{-0.50}$ | 31 |
| Wire chamber, $K^+ p \to K^0 + p + \pi^+$ | 400 | $0.45 \pm 0.35$ | $0.05 \pm 0.35$ | 32 |
| Spark chambers, $\pi^- p \to \Lambda + K^0$ | 99 | $-0.09 \pm 0.19$ | $+0.56 \pm 0.43$ | 33 |
| $\pi^-$ Cu $\to K^0$ | 148 | $-0.05 \pm 0.17$ | $+0.39^{+0.35}_{-0.37}$ | 34 This exp. |
| Average | 1155 | $+0.11 \pm 0.09$ $\chi^2 = 10.0$ with 6 d.f. | $0.24 \pm 0.16$ $\chi^2 = 2.7$ with 7 d.f. | |

with the statistical error. Relative to the best fit, $X = 0$ has a probability of 25%.

The best fit to the final sample of 148 $K \to \pi^+ \pi^- \pi^0$ events gives

$$\mathrm{Re}W = -0.05 \pm 0.17,$$

$$\mathrm{Im}W = +0.39^{+0.35}_{-0.37}.$$

This result is consistent with $CPT$ (Re$W = 0$) and $CP$ invariance ($W = 0$). Again the systematic effects and the backgrounds are small compared to the statistical error. The probability of $W = 0$ is 30% relative to the value of the best fit.

The best compiled value for $X$ indicates that any $\Delta S/\Delta Q$ violation must be small ($\lesssim 0.05$), and is unlikely to be maximal in any sense. The best value for $W$, on the other hand, still allows for substantial $CP$ violation in $K \to 3\pi$ decay.

## ACKNOWLEDGMENTS

We wish to thank the Bevatron operations staff and members of the Lofgren group at the Lawrence Radiation Laboratory at Berkeley for invaluable assistance during the preparation and operation of this experiment at the Bevatron. We gratefully acknowledge the contributions of A. Lake, D. Sell, W. Friedler, H. Grau, S. Sedleniek, and D. Toomer to the design and construction of equipment. D. Chu, P. Walden, K. Young, G. Murata, and J. Stanley assisted in the setup and running stages of the experiment. C. Lam, D. Molodowitch, J. Tam, and L. Young assisted materially in the data analysis. Finally, we acknowledge the skill and perseverance of the scanning and measuring staff under J. Ferrari, including J. Edwards, M. Jolliff, M. Jordan, J. Lyon, and G. Martin.

*Work supported in part by the U. S. Atomic Energy Commission. Prepared under Contract No. AT(11-1)-68 for the San Francisco Operations Office.

†On leave from Imperial College, London, England.

‡Work supported in part by National University of Ireland Traveling Studentship.

§Present address: Department of Physics, Imperial College, London, England.

‖Present address: Department of Physics, University of Illinois, Urbana, Ill.

**Present address: Department of Physics, Hope College, Holland, Michigan.

[1]J. Christenson, J. Cronin, V. Fitch, and R. Turlay, Phys. Rev. Letters 13, 138 (1964).

[2]Particle Data Group, Rev. Mod. Phys. 43, S1 (1971), see p. S15.

[3]T. D. Lee and L. Wolfenstein, Phys. Rev. 138, B1490 (1965).

[4]R. G. Sachs, Phys. Rev. Letters 13, 286 (1964).

[5]S. L. Glashow, Phys. Rev. Letters 14, 35 (1965).

[6]T. D. Lee and C. S. Wu, Ann. Rev. Nucl. Sci. 16, 511 (1966), see p. 564.

[7]N. Cabibbo, *Symmetries in Elementary Particle Physics*, edited by A. Zichichi (Academic, New York, 1964), p. 285.

[8]J. W. Cronin, in *Proceedings of the Fourteenth Inter-*

*national Conference on High Energy Physics, Vienna, 1968,* edited by J. Prentki and J. Steinberger (CERN, Geneva, 1968), p. 285.

[9]$\epsilon = \frac{1}{3}(2\eta^{+-} + \eta^{00})$ [T. D. Lee and C. S. Wu, Ann. Rev. Nucl. Sci. 16, 511 (1966), see p. 530]. Taking the data in Ref. 2 we get $|\epsilon| \approx 2 \times 10^{-3}$. The $|K_L\rangle$ and $|K_S\rangle$ states are defined in terms of $\epsilon$ as follows (assuming *CPT*):

$$|K_S\rangle = [(1+\epsilon)|K^0\rangle + (1-\epsilon)|\bar{K}^0\rangle]/[2(1+|\epsilon|^2)]^{1/2},$$

$$|K_L\rangle = [(1+\epsilon)|K^0\rangle - (1-\epsilon)|\bar{K}^0\rangle]/[2(1+|\epsilon|^2)]^{1/2}.$$

[10]O. I. Dahl, L. M. Hardy, R. I. Hess, J. Kirz, and D. H. Miller, Phys. Rev. 163, 1377 (1967); O. I. Dahl, L. M. Hardy, R. I. Hess, J. Kirz, D. H. Miller, and J. Schwartz, *ibid.* 163, 1430 (1967); 183, 1520(E) (1969).

[11]M. G. Albrow, D. Aston, D. P. Barber, L. Bird, R. J. Ellison, C. Halliwell, R. E. H. Jones, A. D. Kanaris, F. K. Loebinger, P. G. Murphy, M. Strong, J. Walters, A. J. Wynroe, D. D. Yovanovic, and R. F. Templeman, Phys. Letters 33B, 516 (1970).

[12]C. A. Heusch and C. Y. Prescott, IEEE Trans. Nucl. Sci. Vol. NS-12, No. 4, 213 (1965).

[13]T. D. Lee and C. S. Wu, Ann. Rev. Nucl. Sci. 16, 511 (1966), see p. 582.

[14]Particle Data Group, Rev. Mod. Phys. 43, S1 (1971), see p. S13.

$$\tau_S = \frac{1}{\gamma_S} = (0.862 \pm 0.006) \times 10^{-10} \text{ sec},$$

$$\tau_L = (5.172 \pm 0.043) \times 10^{-8} \text{ sec},$$

$$(M_S - M_L) = -(0.5398 \pm 0.0033) \times 10^{10}\, \hbar \text{ sec}^{-1}.$$

[15]B. Aubert, L. Behr, F. L. Canavan, L. M. Chounet, J. P. Lowys, P. Mittner, and C. Pascaud, Phys. Letters 17, 59 (1965).

[16]M. Baldo-Ceolin, E. Calimani, S. Ciampolillo, C. Filippi-Filosofo, H. Huzita, F. Mattioli, and G. Miari, Nuovo Cimento 38, 684 (1965).

[17]P. Franzini, L. Kirsch, P. Schmidt, J. Steinberg, and R. J. Plano, Phys. Rev. 140, B127 (1965).

[18]L. Feldman, S. Frankel, V. L. Highland, T. Sloan, O. B. Van Dyck, W. D. Wales, R. Winston, and D. M. Wolfe, Phys. Rev. 155, 1611 (1967).

[19]Y. Cho, A. Dralle, J. Canter, A. Engler, H. Fisk, R. Kraemer, C. Meltzer, D. G. Hill, M. Sakitt, O. Skjeggestad, T. Kikuchi, D. K. Robinson, and C. Tilger, Phys. Rev. D 1, 3031 (1970).

[20]B. R. Webber, F. T. Solmitz, F. S. Crawford, and M. Alston-Garnjost, Phys. Rev. D 3, 64 (1971).

[21]F. James and H. Briand, Nucl. Phys. B8, 365 (1968).

[22]L. S. Littenberg, J. H. Field, O. Piccioni, W. A. W. Mehlhop, S. S. Murty, P. H. Bowles, and T. H. Burnett, Phys. Rev. Letters 22, 654 (1969).

[23]F. J. Sciulli, J. D. Gallivan, D. M. Binnie, R. Gomez, M. L. Mallary, C. W. Peck, B. A. Sherwood, A. V. Tollestrup, and J. D. van Putten, Phys. Rev. Letters 25, 1214 (1970). This is the result of the $K_{e3}$ measurement reported here. For greater details see J. D. Gallivan, doctoral dissertation, Caltech, 1970 (unpublished).

[24]P. M. Mantsch, A. Abashian, M. F. Graham, L. H. Jones, J. R. Orr, J. H. Smith, R. D. Stutzke, and M. J. Glaubman, Nuovo Cimento 9A, 160 (1972).

[25]G. Neuhofer, F. Niebergall, M. Regler, H. E. Stier, K. Winter, J. J. Aubert, X. DeBouard, V. Lepeltier, L. Massonnet, H. Pessard, M. Vivargent, T. R. Willitts, M. Yvert, W. Bartl, and M. Steuer, in *Proceedings of the Amsterdam International Conference on Elementary Particles, 1971,* edited by M. Veltman (North-Holland, Amsterdam, 1972); K. Winter, CERN Report No. 71-3131 (unpublished).

[26]Y. Cho, A. Dralle, J. Canter, A. Engler, H. Fisk, R. Kraemer, C. Meltzer, D. G. Hill, M. Sakitt, O. Skjeggestad, T. Kikuchi, D. K. Robinson, and C. Tilger, Phys. Rev. D 3, 1557 (1971).

[27]G. W. Meisner, W. A. Mann, S. S. Hertzbach, R. R. Kofler, S. S. Yamamoto, D. Berley, S. P. Yamin, J. Thompson, and W. J. Willis, Phys. Rev. D 3, 59 (1971).

[28]L. Behr, V. Brisson, P. Petiau, E. Bellotti, A. Pullia, M. Baldo-Ceolin, E. Calimani, S. Ciampolillo, H. Huzita, A. Sconza, B. Aubert, L. M. Chounet, J. P. Lowys, and C. Pascaud, Phys. Letters 22, 540 (1966).

[29]J. A. Anderson, F. S. Crawford, R. L. Golden, D. Stern, T. O. Binford, and V. G. Lind, Phys. Rev. Letters 14, 475 (1965); 15, 645 (1965).

[30]B. R. Webber, F. T. Solmitz, F. S. Crawford, and M. Alston-Garnjost, Phys. Rev. D 1, 1967 (1970).

[31]F. James, L. Montanet, E. Paul, E. Pauli, P. Saetre, D. M. Sendall, G. Burgun, E. Lesquoy, A. Muller, S. Zylberajch, and O. Skjeggestad, Phys. Letters 35B, 265 (1971).

[32]J. J. Aubert, G. Neuhofer, F. Niebergall, M. Regler, H. E. Stier, K. Winter, X. DeBouard, V. Lepeltier, L. Massonnet, H. Pessard, M. Vivargent, T. R. Willitts, M. Yvert, W. Bartl, and M. Steuer, in *Proceedings of the Amsterdam International Conference on Elementary Particles, 1971,* edited by M. Veltman (Ref. 25).

[33]L. H. Jones, A. Abashian, M. F. Graham, P. M. Mantsch, J. R. Orr, J. H. Smith, R. D. Stutzke, and M. J. Glaubman, Nuovo Cimento 9A, 151 (1972).

[34]M. L. Mallary, doctoral dissertation, Caltech, 1971 (unpublished).